10 YEARS ANNIVERSARY

INORGANIC CHEMISTRY

FRONTIERS

RESEARCH ARTICLE

Check for updates

An in solution adsorption characterization technique based on the response to an external magnetic field of porous paramagnetic materials: application on supramolecular metal–adenine frameworks containing heterometallic heptameric clusters†

Jon Pascual-Colino, ‡[a] Rubén Pérez-Aguirre,‡[a,b] Garikoitz Beobide, [a,c] Oscar Castillo, *[a,c] Imanol de Pedro,[b] Antonio Luque, [a,c] Sandra Mena-Gutiérrez [a] and Sonia Pérez-Yáñez [c,d]

Herein we explore the opportunities arising from combining magnetic properties and porosity in metal–organic materials. In this sense, we have prepared an adenine based homometallic wheel-shaped heptameric $[Cu_7(\mu\text{-adeninato})_6(\mu_3\text{-OH})_6(\mu\text{-OH}_2)_4]^{2+}$ entity containing two metal coordination environments: CuO_6 at the core of the wheel with an unusually modest Jahn–Teller distortion and six peripheral CuN_2O_4 with a more pronounced elongation. The difference in the coordination environments of this compound facilitates the selective replacement of the central metal position by other metal centers (Zn^{II}, Ni^{II}, Co^{II} and Cr^{III}) and boosts the magnetic properties of the homometallic heptameric entity. The nature of the central metal modulates the complex net of ferro- and antiferromagnetic superexchange pathways within the heptameric entity to tune the total spin (S_T = 3 (**Cu₆Zn**), 5/2 (**Cu₆Cu**), 2 (**Cu₆Ni**), 3/2 (**Cu₆Co**), and 9/2 (**Cu₆Cr**)). No evidence of single-molecule magnet behavior has been observed at 2 K, but at room temperature, where these compounds are still in the paramagnetic regime, the attraction force exerted by an external magnetic field (H) on particles immersed in a liquid is enough to keep them attached to an electromagnet pole. The $4S(S + 1)$ value of the central metal follows a linear dependence with respect to the $1/[H \cdot \nabla(H)]$ value at which the particles are detached from the pole of the electromagnet. There is also a linear dependence of the $H \cdot \nabla(H)$ term with respect to the adsorbate mass incorporated inside the pores of the paramagnetic adsorbent which has allowed performing straightforward sorption selectivity experiments on **Cu₆Cu** directly in solution, which are based on a property of the adsorbent and not as usually based on an indirect assessment of the adsorbate remaining in solution.

[a]*Departamento de Química Orgánica e Inorgánica, Facultad de Ciencia y Tecnología, Universidad del País Vasco/Euskal Herriko Unibertsitatea, UPV/EHU, Apartado 644, E-48080 Bilbao, Spain. E-mail: oscar.castillo@ehu.eus*
[b]*CITIMAC, Facultad de Ciencias, Universidad de Cantabria, E-39005 Santander, Spain*
[c]*BCMaterials, Basque Center for Materials, Applications and Nanostructures, UPV/EHU Science Park, E-48940 Leioa, Spain*
[d]*Departamento de Química Orgánica e Inorgánica, Facultad de Farmacia, Universidad del País Vasco/Euskal Herriko Unibertsitatea, UPV/EHU, E-01006 Vitoria-Gasteiz, Spain*
†Electronic supplementary information (ESI) available: Films describing the magnetic sustentation experiment, details of FTIR spectroscopic data, thermogravimetric measurements, X-ray photoelectronic spectroscopy data, and crystallographic and structural data. CCDC 2153696–2153698. For ESI and crystallographic data in CIF or other electronic format see DOI: https://doi.org/10.1039/d2qi01994a
‡These authors contributed equally.

Introduction

There is great interest in developing polynuclear transition metal entities with a high total magnetic spin state as they are potential sources of single-molecule magnets and also show a broad scope of potential applications.[1–5] In these efforts, one of the most successful strategies relies on the combination of a central paramagnetic metal atom connected to an external collection of surrounding paramagnetic metal centers through bridging ligands with a great ability to mediate strong magnetic interactions (cyanido, oxalato, oxido, and hydroxido).[6] A very successful strategy has been capping growing metal oxide entities with carboxylic ligands to limit its polymerization. The first example of this kind of material is the Mn₁₂–acetate species, a prototypical single molecule magnet.[7] There are

2250 | *Inorg. Chem. Front.*, 2023, **10**, 2250–2261

This journal is © the Partner Organisations 2023

some other examples following this approach but they are limited to oxophilic transition metals such as manganese and iron, providing in this way very robust polynuclear discrete entities with single molecule magnet behaviour coming from the great anisotropy of these ions.[8] On the other hand, the anti–anti coordination mode of the carboxylate is similar and can be replaced by the μ-$\kappa N3$:$\kappa N9$ coordination mode of the adenine nucleobase providing access to a similar capping approach but in less oxophilic transition metals such as those at the right end of d-block. We have proved that the use of the adenine nucleobase with copper under basic conditions promotes the formation of heptanuclear discrete copper-hydroxido entities capped by the adeninato ligands ([Cu$_7$(μ-adeninato)$_6$(μ_3-OH)$_6$(μ-OH$_2$)$_6$]$^{2+}$).[9–11] The coordination environment of the central position with a reduced Jahn–Teller distortion makes it suitable for metal replacement allowing us to obtain a family of heptameric entities: [Cu$_6$M(μ-adeninato)$_6$(μ_3-OH)$_6$(μ-OH$_2$)$_4$]SO$_4$ with M^{II}: Cu and Ni, and [Cu$_6$M(μ-adeninato)$_6$(μ_3-OH)$_6$(μ-OH$_2$)$_6$](SO$_4$)$_x$ with M^{II} (with x = 1): Zn, Co and M^{III} (with x = 1.5): Cr.

Coming back to the magnetic properties, it is well known that bridging ligands play a key role in determining the strength and nature of the superexchange magnetic interaction, but the nature of these interactions can also be modulated by the careful selection of the paramagnetic centers. In this sense, the antiferromagnetic interactions for overlapping magnetic orbitals can flip to the ferromagnetic nature when those magnetic orbitals are orthogonal.[12,13] In fact, in this work we use extensively this strategy to obtain a great variety of magnetically ordered ground state total spins: from 3/2 to 9/2.

Usually, the reported studies on this kind of material are focused on the analysis of their magnetic ordering that takes place well below room temperature.[6,14] However, the generation of a high total magnetic spin state does not necessarily imply a single-molecule magnet behaviour as great magnetic anisotropy is required among other parameters.[15] Instead of that, we herein address the challenge of using the room temperature paramagnetic response of this kind of compound towards an external magnetic field to prompt a driven motion of its particles while immersed in a liquid and even to accomplish sensing through the quantification of this response. Related to the latter, recently we have reported the use of the compound [Cu$_6$Cr(μ-adeninato)$_6$(μ_3-OH)$_6$(μ-OH$_2$)$_6$](SO$_4$)$_{1.5}$, **Cu$_6$Cr**, to capture anti-inflammatory anionic drugs from aqueous effluents and to quantify them through this new magnetic sensing approach.[16] In this work, we are focused on performing a more specific sorption selectivity study using a broader selection of adsorbates. It is also aimed to determine experimentally the dependence that the response toward an external magnetic field has with respect to the paramagnetic centers incorporated in the heptameric entity as within the [Cu$_6$M(μ-adeninato)$_6$(μ_3-OH)$_6$(μ-OH$_2$)$_6$](SO$_4$)$_x$ compounds all other parameters that could have an impact on this response are almost equalized.

Experimental

Synthetic procedures

Synthesis of [Cu$_6$Zn(μ-adeninato-$\kappa N3$:$\kappa N9$)$_6$(μ_3-OH)$_6$(μ-OH$_2$)$_6$]SO$_4$·32H$_2$O (Cu$_6$Zn). 20 mL of an aqueous solution of copper(II) sulfate pentahydrate (0.8 mmol, 0.200 g) and zinc(II) sulfate pentahydrate (0.2 mmol, 0.055 g) were poured into 20 mL of a hot water/methanol solution containing adenine (0.8 mmol, 0.108 g). The pH of the resulting light blue suspension (pH = 3.1) was shifted to 8.5 by adding dropwise 1 M solution of sodium hydroxide. The reaction mixture was left evaporating at room temperature in a crystallizer sealed with a sealing film (Parafilm^{TM}) slightly holed to allow slow solvent evaporation. Six days later, needle-like light blue crystals were formed. Yield: 55% (based on copper). Main IR features (cm^{-1}; KBr pellets): 3400vs, 3200sh, 1640s, 1610vs, 1550s, 1465m, 1400m, 1305m, 1270m, 1195m, 1150m, 1110m, 1030w, 935w.

Synthesis of [Cu$_7$(μ-adeninato-$\kappa N3$:$\kappa N9$)$_6$(μ_3-OH)$_6$(μ-OH$_2$)$_4$] SO$_4$·20H$_2$O (Cu$_6$Cu). Adenine (0.8 mmol, 0.108 g) was dissolved in 20 mL of a water–methanol mixture in a 1:1 ratio under continuous stirring and heating. Thereafter, it was added to an aqueous solution of 20 mL of copper(II) sulfate pentahydrate (0.8 mmol, 0.200 g). The appearance of a bluish suspension was observed at pH = 2.9. The suspension was redissolved by adding sulfuric acid dropwise to pH = 1.8. Then, 1 M sodium hydroxide was added dropwise obtaining a new dark blue suspension (pH = 10.1) that was placed in a small beaker and introduced into an Erlenmeyer flask containing a 1/5 (v/v) sulfuric acid solution. The vapor diffusion taking place inside the closed Erlenmeyer flask acidified the solution slowly. After four days, blue cubic crystals of **Cu$_6$Cu** were obtained (pH = 9.1). Yield: 60%. Main IR features (cm^{-1}; KBr pellets): 3430vs, 3420sh, 1640s, 1605vs, 1545s, 1465m, 1400m, 1305m, 1275m, 1200m, 1150m, 1110m, 1030w, 935w.

Synthesis of compound [Cu$_6$Ni(μ-adeninato-$\kappa N3$:$\kappa N9$)$_6$(μ_3-OH)$_6$(μ-OH$_2$)$_4$]SO$_4$·14H$_2$O (Cu$_6$Ni). Adenine (0.8 mmol, 0.108 g) and nickel(II) chloride (0.2 mmol, 0.048 g) were added into a solution of 20 mL of methanol/water (1:1 volume ratio), heating it up under continuous stirring until a green solution was obtained. To that, 20 mL of an aqueous solution of copper(II) sulfate pentahydrate (0.8 mmol, 0.200 g) was added, obtaining a bluish suspension with pH = 3.3 which was acidified with sulfuric acid until it was completely dissolved (pH = 2.1) into a light green solution. Thereafter, triethylamine was added until the formation of a blue-green suspension at pH = 9.5 which was transferred to a crystallizer covered with a sealing film. After two days, rectangular blue crystals were obtained. Yield: 55%. Main IR features (cm^{-1}; KBr pellets): 3335vs, 3200sh, 1640s, 1600vs, 1545s, 1465m, 1395m, 1305m, 1275m, 1200m, 1150m, 1110m, 1030w, 935w.

Synthesis of [Cu$_6$Co(μ-adeninato-$\kappa N3$:$\kappa N9$)$_6$(μ_3-OH)$_6$(μ-OH$_2$)$_6$] SO$_4$·35H$_2$O (Cu$_6$Co). An aqueous solution containing copper(II) sulfate pentahydrate (0.8 mmol, 0.200 g) and cobalt(II) sulfate heptahydrate (0.2 mmol, 0.056 g) was added to a solution of adenine (0.8 mmol, 0.108 g) in 20 mL of methanol/water (1:1 volume ratio), heating under continuous stirring. After

This journal is © the Partner Organisations 2023

Inorg. Chem. Front., 2023, **10**, 2250–2261 | **2251**

10 minutes, the reaction mixture was left to temper, obtaining a blue suspension with pH = 3.78 which was left stirring for one hour (the colour turns to violet). Then, sodium hydroxide (1 M) was added dropwise until a pH value of 10.1 is reached. Finally, the resulting suspension was placed into a crystallizer covered with a sealing film and left in a fridge at 6 °C. After five days, blue needle-shaped crystals were obtained. Yield: 65%. Main IR features (cm^{-1}; KBr pellets): 3335vs, 3200sh, 1640s, 1600vs, 1545s, 1465m, 1395m, 1305m, 1275m, 1200m, 1150m, 1110m, 1030w, 935w.

Synthesis of [Cu$_6$Cr(μ-adeninato-κN3:κN9)$_6$(μ$_3$-OH)$_6$(μ-OH$_2$)$_6$] (SO$_4$)$_{1.5}$·17H$_2$O (Cu$_6$Cr). The synthesis was performed as previously reported.[16]

Characterization

General characterization techniques. The IR spectra (KBr pellets) were recorded on a FTIR 8400S Shimadzu spectrometer in the 4000–600 cm^{-1} spectral region. Variable-temperature magnetic susceptibility measurements were performed using a standard Quantum Design PPMS magnetometer whilst heating from 2 to 300 K at 1 kOe range after cooling in the absence (zero field cooling, ZFC) of the applied field. Magnetization as a function of field (H) was measured using the same magnetometer in the range of −50 ≤ H/kOe ≤ 50 at 2 K after cooling the sample in zero field. The susceptibility data were corrected for the diamagnetism estimated from Pascal's tables,[17] the temperature-independent paramagnetism and the magnetization of the sample holder. Thermal analyses (TG/DTA) were performed on a METTLER TOLEDO TGA/SDTA851 thermal analyzer in a synthetic air (79% N$_2$/21% O$_2$) flux of 50 cm^3 min^{-1} with a heating rate of 5 °C min^{-1}. Magnetic sustentation experiments were performed using a Newport Pagnell England Electromagnet Type C sourced with a Hewlett Packard 6655A System DC Power Supply to provide a variable magnetic field under which the particles of the compound dispersed in water are attached to the lower end of the electromagnet pole until the magnetic field decreases enough for the gravitation to prevail and the particles to fall down. The ^{1}H-NMR spectra were acquired in a Bruker AVANCE 500 (one-bay; 500 MHz) at 293 K. The purity of the samples was assessed by powder X-ray diffraction, thermogravimetry and FTIR analysis. The powder X-ray diffraction (PXRD) patterns were collected on a Philips X'PERT powder diffractometer with Cu Kα radiation (λ = 1.5418 Å) over the 5 < 2θ < 70° range with a step size of 0.02° and an acquisition time of 2.5 s per step at 25 °C. See further details in the ESI.†

Single-crystal X-ray determination. Single-crystal X-ray diffraction data were collected at 100(2) K on an Agilent Technologies Supernova diffractometer. The data reduction was done with the CrysAlisPro program.[18] Crystal structures were solved by direct methods using the SIR92 program[19] and refined by full-matrix least-squares on F^2 including all reflections (WINGX).[20,21] In all compounds some of the adeninato ligands are disordered into two arrangements with inverted orientation regarding the coordination mode (μ-κN3:κN9/μ-κN9:κN3).[22,23] Furthermore, in compound **Cu$_6$Co** several

restraints (DFIX and FLAT) were required to retain the expected geometry of the adeninato ligands. In all these crystal structures the sulfate counterions are disordered over several positions related by the symmetry elements. The crystal structure of these compounds revealed the presence of large channels in which the solvent molecules are placed. The high disorder that these molecules show precluded their modeling and, as a consequence, the electron density at the voids of the crystal structure was subtracted from the reflection data by the SQUEEZE method[24] as implemented in the PLATON.[25] Details of the structure determination and refinement of compounds **Cu$_6$Zn**, **Cu$_6$Cu** and **Cu$_6$Co** are summarized in Table S3.† As it was not possible to obtain single crystals of the **Cu$_6$Ni** compound its structural characterization was performed by XRPD. Indexation of its diffraction profile was carried out using the FULLPROF program[26] on the basis of the space group and cell parameters found for isostructural **Cu$_6$Cu**, providing the following unit cell parameters: Cccm, a = 10.559(1) Å, b = 25.048 (2) Å and c = 27.301(4) Å. See further details in the ESI.†

Sorption quantification by ^{1}H-NMR. The ^{1}H-NMR spectra were acquired in a Bruker AVANCE 500 (one-bay; 500 MHz) at 293 K. The sorption experiment was repeated but using D$_2$O: 15 mg of compound **Cu$_6$Cu**, 1.5 mL of deuterated water D$_2$O and 15 mg of the adsorbate of interest (aniline, ribose, glucose or sucrose). The samples were left under continuous stirring for 24 h under room conditions (25 °C). Later 15 μL of isopropanol were added and immediately the sample was filtered to separate the solid from the solution. The same procedure was applied for each adsorbate but without adding the porous material (**Cu$_6$Cu**) in order to set the initial adsorbate amount in the sorption experiment. ^{1}H-NMR measurement was performed on the filtered solution and the characteristic signals of the adsorbate and isopropanol were employed to quantify the amount of it remaining in solution and with their difference from the initial value to determine the amount adsorbed within the porous material. See further details in the ESI.†

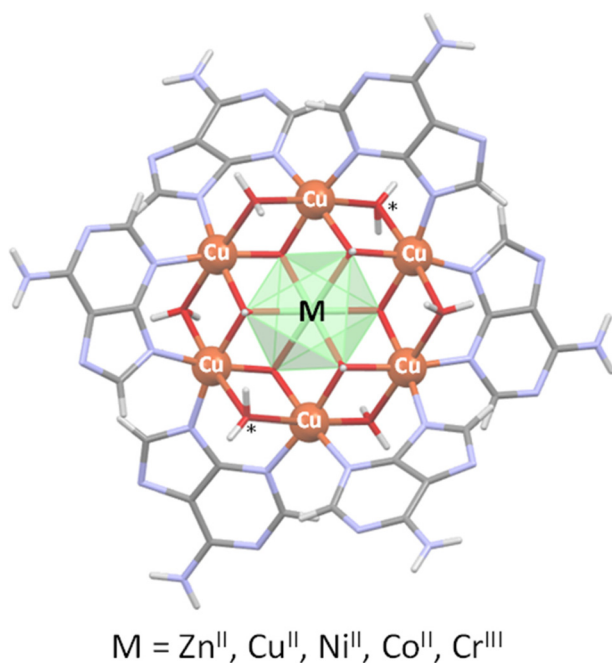## Results and discussion

Crystal structure determination

Single crystal X-ray diffraction data allowed us to elucidate the crystal structure of the compounds.§ In previous works we have designed and characterized several supramolecular metal–organic frameworks containing a wheel shaped heptameric [Cu$_7$(μ-adeninato)$_6$(μ$_3$-OH)$_6$(μ-OH$_2$)$_6$]$^{2+}$ entity whose positive charge is counterbalanced by inorganic (sulfate) or organic species (theobrominate, terephthalate and benzoate).[9–11] Both types of counterions can play a role in the

---

§ Crystallographic data. **Cu$_6$Zn**: crystal system: trigonal; space group: R$\bar{3}$c; cell parameters: a = b = 19.108(1) Å, c = 43.046(3) Å and V = 13611(2) Å^3. **Cu$_6$Cu**: crystal system: orthorhombic; space group: Cccm; cell parameters: a = 10.5080(3) Å, b = 24.8920(8) Å, c = 27.0312(9) Å, and V = 7070.4(4) Å^3. **Cu$_6$Co**: crystal system: trigonal; space group: R$\bar{3}$c; cell parameters: a = b = 19.058(3) Å, c = 43.157(9) Å and V = 13 575(5) Å^3. See the ESI† for further details.

2252 | *Inorg. Chem. Front.*, 2023, **10**, 2250–2261
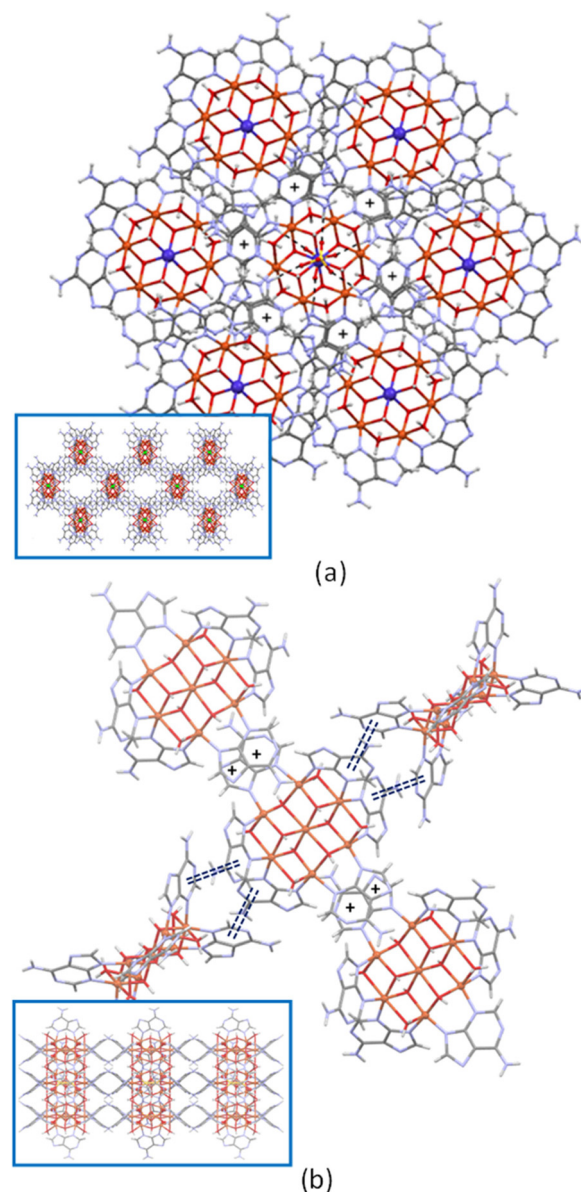
This journal is © the Partner Organisations 2023

supramolecular forces (hydrogen-bonding and π-stacking interactions) that govern the overall crystal packing but they have little impact on the magnetic behaviour, which is greatly dominated by the superexchange pathways within the discrete heptameric entities and only at very low temperatures (below 5 K) some differences arise from the far more weaker superexchange pathways involving the dissimilar supramolecular interactions. A closer analysis of the discrete heptameric $[Cu_7(\mu\text{-adeninato})_6(\mu_3\text{-OH})_6(\mu\text{-OH}_2)_6]^{2+}$ entity revealed the presence of two types of metal coordination environments, a $Cu(OH)_6$ chromophore at the core of the wheel with an unusually modest Jahn–Teller distortion and the six peripheral $CuN_2(OH)_2(Ow)_2$ environments with the common and pronounced Jahn–Teller distortion affecting the coordinated water molecules. This feature suggested us the possibility of replacing central copper(II) by other transition metal ions with a usually more regular coordination environment, in this way, to tune the magnetic properties of the heptameric entity. A recent work in which this central position was replaced by a Cr^{III} atom (**Cu₆Cr**) confirms the suitability of this approach.[16] Now, we report herein four compounds, the homometallic $[Cu_7(\mu\text{-adeninato-}\kappa N3{:}\kappa N9)_6(\mu_3\text{-OH})_6(\mu\text{-OH}_2)_4](SO_4){\cdot}nH_2O$ compound (**Cu₆Cu**), and heterometallic $[Cu_6M(\mu\text{-adeninato-}\kappa N3{:}\kappa N9)_6(\mu_3\text{-OH})_6(\mu\text{-OH}_2)_6](SO_4){\cdot}nH_2O$; M^{II}: Zn (**Cu₆Zn**), Ni (**Cu₆Ni**), Co (**Cu₆Co**). Fig. 1 shows a schematic representation of the discrete heptameric units in which the connectivity is essentially identical, in such a way that a central $[M^{II}(OH)_6]^{4-}$ or $[M^{III}(OH)_6]^{3-}$ core (**Cu₆Cr**) is connected to the six copper(II) metal centers comprising the external ring. The peripheral copper atoms are further connected among them through the

double μ-H_2O and six μ-adeninato-$\kappa N3{:}\kappa N9$ bridges. It is necessary to note that in homometallic **Cu₆Cu**, two water molecules, labelled as * in Fig. 1, are not present owing to the arrangement of the adjacent adeninato ligands that precludes their attachment.

Regarding the self-assembly of the heptameric cations in the crystal packing, two basic arrangements are observed (Fig. 2). Each entity, in the trigonal $R\bar{3}c$ **Cu₆Zn** and **Cu₆Co** compounds, is six-connected by means of π–π interactions (comprising its six adeninato ligands) to three upper and to three lower ones to give a **pcu** topology with a $4^{12}{\cdot}6^3$ point symbol.[27] In **Cu₆Cu** and **Cu₆Cr** compounds, the complex entities are four connected by single π–π stacking interactions with

Fig. 1 Heptameric clusters depicting the targeted replacement of the central metal center. Symbol "*" indicates the absent coordination water molecules in compound **Cu₆Cu**.

Fig. 2 Details of the π-stacking interactions (+ symbol and double dashed lines) in compounds **Cu₆Zn** (a) and **Cu₆Cu** (b). The insets show a projection of the crystal packing.

two adjacent polynuclear entities and by double π–π stacking interactions with another two ones that require the interacting entities to be perpendicularly oriented among them.

However, there is a subtle difference on the single π–π stacking interaction: the face exposed by the adeninato ligands for this interaction is at the side of the hydroxido ligand bridging the same metal centers in **Cu₆Cr** whereas it employs the other face in **Cu₆Cu**. This fact is at the bottom of their different space group and topology. **Cu₆Cu** and **Cu₆Ni** crystallize in the orthorhombic *Cccm* space group and present an **sql**/Shubnikov tetragonal plane net topology with a $4^4 \cdot 6^2$ point symbol, whereas **Cu₆Cr** belongs to the monoclinic *C*2/*c* space group and it shows a **cds** CdSO₄ like topology with a $6^5 \cdot 8$ point symbol.[27]

The sulfate anions are inserted in the cavities left by the π–π arrangement of the discrete heptameric entities and do not play a crucial role in directing the crystal packing, but provide mere counterbalance of the charge of the cationic entities. Each sulfate anion in **Cu₆Co**, with a S–O bond lying in a three-fold axis, is hydrogen bonded like a tripod to three OH groups of the heptameric cation, whereas in the isostructural **Cu₆Zn** compound the disposition of the sulfate anion differs, with only one of the sulfate O-atoms placed on the ternary axis (Fig. 3). In the **Cu₆Cr** compound, the sulfate arrangement is similar to **Cu₆Zn**, but the total site occupancy for each sulfate is set to 1/2 to counterbalance the charge of the complex entity.

The above-described supramolecular assembling of cations and anions in all the compounds leads to a three-dimensional crystal packing with channels that occupy a very significant percentage of the total unit cell volume: from 32% (**Cu₆Cu**) to 51% (**Cu₆Zn**). These channels are occupied by crystallization water molecules. The innocent structural role of the sulfate anions, the high tendency of the heptameric cation to form crystal networks sustained by supramolecular adeninato⋯ adeninato π–π interactions, and the intrinsic porosity of these networks suggest the insertion of other guest molecules as feasible, as corroborated by the fact that the trigonal **Cu₆Zn** and **Cu₆Co** compounds present the same space group and a very similar cell parameters to those of the previously reported
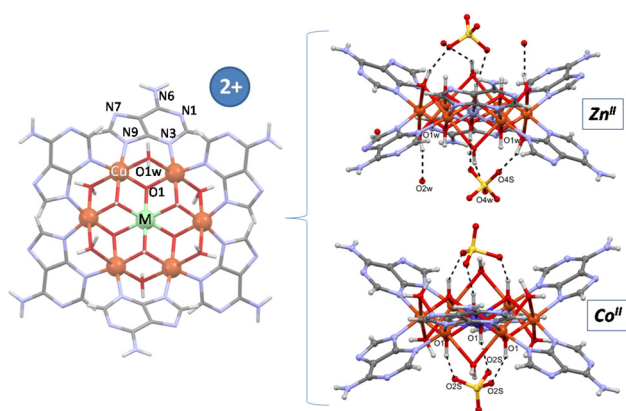
[Cu₇(μ-adeninato-κ*N3*:κ*N9*)₆(μ₃-OH)₆(μ-OH₂)₆](NHEt₃)₂(SO₄)₂· 23H₂O compound, whereas monoclinic **Cu₆Cr** is isostructural with the [Cu₇(μ-adeninato-κ*N3*:κ*N9*)₆(μ₃-OH)₆(μ-OH₂)₆] (NHEt₃)₂(SO₄)₂·42H₂O compound.[9] Both compounds show the co-crystallization of the (NHEt₃)₂(SO₄) salt inside the channels of the supramolecular network of the heptameric cations without modifying it.
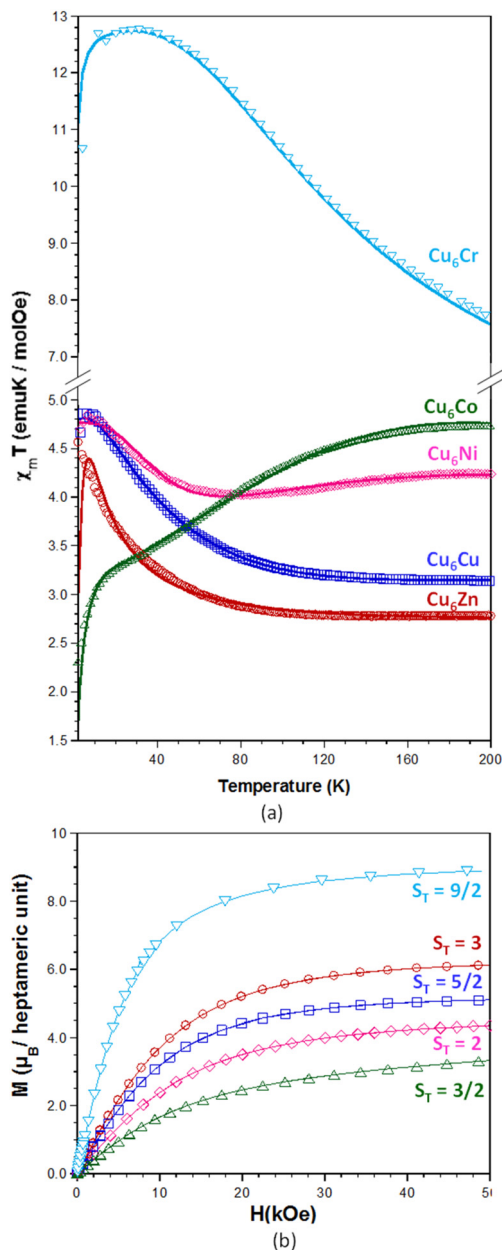
Magnetic characterization

Fig. 4 shows the thermal dependence of the $\chi_M T$ product measured at 1 kOe after cooling without an applied magnetic field (ZFC) and the magnetization curves at 2 K for compounds **Cu₆M**. Data corresponding to previously published **Cu₆Cr** have been included for comparative purposes.[16]

The experimental $\chi_M T$ values at 300 K agree with those values calculated for magnetically non interacting six Cu(ɪɪ) and one central M^{III} or M^{II} atoms, indicating that these compounds are still within the paramagnetic regime at room temperature with the exception of compound **Cu₆Cr** which shows a slightly higher and not constant value of $\chi_M T$ near room temperature. On the other hand, the thermal evolution of the $\chi_M T$ products and the S_T value observed in the magnetization curves make clear that compounds **Cu₆Zn** and **Cu₆Cr** are ferromagnetic whereas compounds **Cu₆Cu**, **Cu₆Ni** and **Cu₆Co** are ferrimagnetic, in good agreement with the magnetic ordering and magnetic superexchange pathways depicted in Fig. 5.

Moreover, a slight decrease of the $\chi_M T$ product to below 5 K happens, which has been attributed to the presence of very weak intermolecular antiferromagnetic superexchange pathways mediated by the supramolecular interactions that hold the heptameric entities together. In the case of compound **Cu₆Co**, which presents a more accused decrease, this behaviour can be explained by the presence of a ground state zero-field splitting of cobalt(ɪɪ) ion due to its great orbital contribution[28–30] that it is added to the previously described intermolecular antiferromagnetic interactions. The magnetization curves at 2 K do not show hysteresis indicative of the absence of single-molecule magnet behaviour up to this temperature, despite the non-zero spin ground state. A fitting of the $\chi_M T$ curves above 10 K was performed using the MagProp software tool distributed with the DAVE.[31] The resulting magnetic coupling constants (Table 1) for the superexchange magnetic pathways depicted in Fig. 5 are in concordance with the expectations on the magnetic topology inferred from the saturation magnetization of **Cu₆M** clusters. The magnetic data fitting of **Cu₆Co** has not been performed because the complexity of the cobalt(ɪɪ) magnetic behaviour would require the introduction of additional parameters that would lead to an over parametrization of the system.

In all compounds, the external superexchange interaction between the Cu^{II} ions bridged by μ-adeninato and μ₃-OH bridges (J_1) results in ferromagnetic values. Usually, the presence of both non-linear NCN bridges and wide angle μ-hydroxido bridges (*ca.* 104°) cause strong antiferromagnetic couplings.[32,33] However, the coexistence of these two types of bridges connecting the same metal centers counterbalances
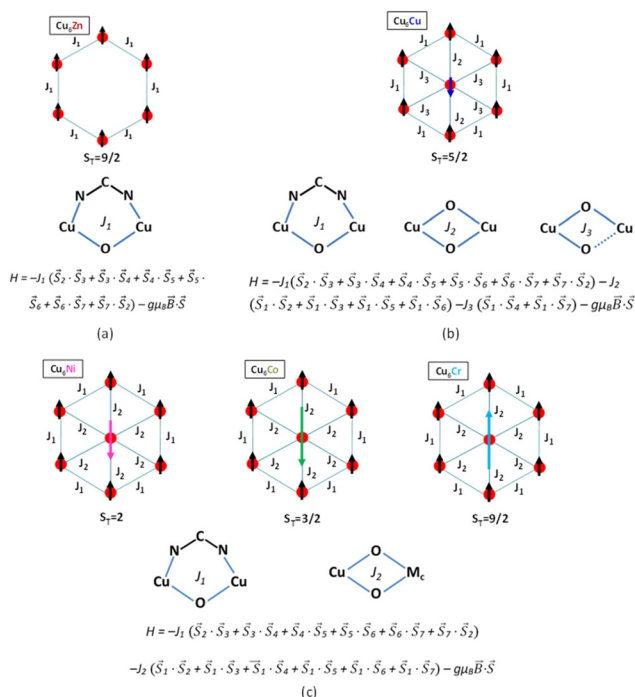

Fig. 3 Heptameric cluster and disposition of sulfate counterions for compounds **Cu₆Zn** and **Cu₆Co**.

2254 | *Inorg. Chem. Front.*, 2023, **10**, 2250–2261

This journal is © the Partner Organisations 2023

Fig. 4 (a) Thermal evolution of the $\chi_M T$ products with the best fitting theoretical models depicted as a continuous line. (b) Magnetization curves at 2 K.

Fig. 5 Ground state of the magnetic ordering at low temperature and the phenomenological Hamiltonian employed for modeling the super-exchange interactions of the heptameric entities with a diamagnetic metal center (a) and with paramagnetic ones (b and c).

Table 1 Best fitting parameters of the magnetic susceptibility curves[a]

	J_1	J_2	J_3	zJ'	$S_{T\,(2\,K)}$
Cu₆Zn	+18	—	—	−0.36	3
Cu₆Cu	+97	−212	+49	−0.03	5/2
Cu₆Ni	+47	−31	—	—	2
Cu₆Cr	+80	+50	—	−0.02	9/2

[a] J_{1-3} (cm^{-1}).

their effects.[34–36] In fact, the splitting of the molecular magnetic orbitals is reversed for each type of bridging ligand (orbital counter-complementarity), thus leading to an almost negligible energy difference between them and, as a consequence, to the observed ferromagnetic interaction.

The radial magnetic pathway J_2, involving double short coordination bond distance μ-OH bridges, depends on the nature of the central metal ion. In **Cu₆Zn**, the diamagnetic nature of Zn(II) simplifies the magnetic superexchange pathways solely to external J_1 and thus, it provides a ferromagnetic compound with $S_T = 3$. In compounds **Cu₆Ni**, **Cu₆Co** and **Cu₆Cr** with paramagnetic metal centers, the nature of the mag-

netic orbitals determines the parallel or antiparallel alignment between the magnetic spins of the peripheral and central paramagnetic centres. In the case of **Cu₆Cr**, a total spin of 9/2 results from a ferromagnetic interaction of the central chromium(III) ion with the ferromagnetically coupled Cu₆-ring. The ferromagnetic nature of this coupling is expectable considering the orbital orthogonality taking place between copper(II) (e_g) and chromium(III) (t_{2g}) magnetic orbitals. In compounds **Cu₆Co** and **Cu₆Ni**, the presence of e_g symmetry magnetic orbitals ensures an efficient overlap through the hydroxido bridges and an antiferromagnetic coupling leading to $S_T = 3/2$ and 2, respectively.[37–40] The superexchange magnetic pathways in **Cu₆Cu** are more complex due to the Jahn–Teller tetragonal elongation present in the central copper(II) atom. The simplest Hamiltonian describing the magnetic behaviour of this compound involves an additional third superexchange magnetic pathway (J_3; see Fig. 5b). J_3 involves a mixture of equatorial–equatorial (short–short) and equatorial–axial (short–long) co-

This journal is © the Partner Organisations 2023

Inorg. Chem. Front., 2023, **10**, 2250–2261 | **2255**

ordinated μ-OH bridges, whereas, as previously stated J_2 presents only an equatorial–equatorial (short–short) arrangement of the bridging hydroxide ligands. The antiferromagnetic nature of J_2 agrees with that stated by Hatfield *et al.* for symmetrically double bridged hydroxido dinuclear complexes, in which angles larger than 98.5° promote an antiferromagnetic coupling.[41] On the other hand, the weak ferromagnetic J_3 interaction is related to the orthogonality between the magnetic orbitals imposed by the combination of symmetric and asymmetric μ-OH bridges. According to previous results, copper(II) centres bridged by this arrangement of the hydroxide bridges usually show a ferromagnetic behaviour with J values ranging from +10 to +90 cm^{-1}.[42] As a consequence of the presence of these three magnetic pathways, a spin frustration situation arises as there is no optimal spin ordering within the heptameric entity that could fulfill all the magnetic interaction preferences. The relative strength of these pathways: $|J_2(\text{antiferromagnetic})|$, $|J_1(\text{ferromagnetic})|$ > $|J_3(\text{ferromagnetic})|$ determines a S_T = 5/2 ground state as observed in its magnetization curve at 2 K.

Magnetic sustentation experiments

As previously stated, these compounds establish complex magnetic interactions at low temperatures, but at room temperature they are well placed in the paramagnetic regime as it can be deduced from their $\chi_M T$ product at room temperature with the exception of **Cu$_6$Cr** as mentioned previously. Therefore, the attraction force exerted by a relatively strong external magnetic field (*i.e.* that of magnets or electromagnets) on the particles of the samples is not strong enough to overcome the earth gravity attraction under normal conditions and, as a consequence, no displacement takes place on these particles. Contrarily, under attenuated gravity force, such as it occurs for particles suspended in a liquid, the magnetic field attraction is capable to sustain the particles avoiding their deposition at the bottom and even to induce their motion upon magnetic field shifts (Fig. 6). In this sense, a double pole electromagnet was employed in order to get fine control over the applied
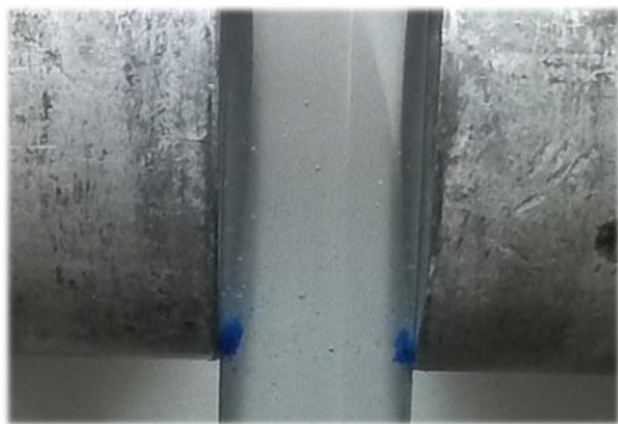

Fig. 6 **Cu$_6$Zn** particles attached to the poles of the electromagnet while submerged in water.

magnetic field. The equation that accounts for the attraction between the paramagnetic particles and the magnetic field is: $F = \nabla(m \cdot H)$, where the gradient ∇ is the change of the quantity $m \cdot H$ per unit distance (m: magnetic dipole of the particle and H: external magnetic field), and the direction is that of the maximum increase of $m \cdot H$. If m is aligned with H, as it is the case for paramagnetic particles, the gradient brings the particles towards the regions of maximum H-field.

The paramagnetic nature of the particles implies that their magnetic dipole is related to the external magnetic field and assuming the particles are small, it can be considered constant and taken away from the gradient (eqn (1)):

$$F_P = m \cdot \nabla(H_P) = \mu_0 \frac{\chi_M}{MW} \cdot \rho_P \cdot V_P \cdot H \cdot \nabla(H_P) \qquad (1)$$

where F_P is the magnetic attraction force on the particle, μ_0 is the permeability of vacuum, χ_M is molar susceptibility, MW is the molecular weight of the compound framework (excluding the solvent molecules hosted in the pores), ρ_P is the density of the compound framework, V_P is the particle volume occupied by the framework (excluding the pore volume), H and $\nabla(H_P)$ are the magnetic field and field gradient in the centre of the particle.

The magnetic force on the particles is not uniform on the whole surface of the pole but it becomes the maximum at the edge, because of the maximum magnetic field gradient placed there. Therefore, the particles are going to accumulate preferentially at this position where the magnetic attraction force is opposite to the gravitation force (Fig. 6).

The use of an electromagnet that allows dialling the magnetic field at the expense of the experimentalist facilitates determining the critical magnetic field at which the particles fall from the pole bottom edge. The molecular susceptibility can be estimated, in a first approximation, using spin-only expression depicted using eqn (2):

$$\chi_M = \frac{[4S_M(S_M + 1)] + 6 \cdot [4S_{Cu}(S_{Cu} + 1)]}{8T} \qquad (2)$$

Considering eqn (1) and (2), and having in mind that the buoyancy force exerted by the solvent on the particles applies only to the compound framework (not to the volume occupied by the pores of the material, as the solvent molecules placed there freely exchange with the solution molecules), the mentioned critical magnetic field can be calculated from the following expression (3):

$$\mu_0 \frac{[4S_M(S_M + 1)] + 6 \cdot [4S_{Cu}(S_{Cu} + 1)]}{8T \cdot MW} \\ \cdot \rho_P \cdot V_P \cdot H \cdot \nabla(H_P) = (\rho_P - \rho_S) \cdot V_P \cdot g \qquad (3)$$

where ρ_S is the solvent density and g is the gravity of Earth. At this point, it is necessary to perform two approximations in order to simplify the previous equation. The first one relies on the molecular mass similarity of the most of the compounds reported herein (see Table 2), which allows us to assume that the MW parameter remains essentially constant. The same applies for the density of the compound framework (ρ_P).

2256 | *Inorg. Chem. Front.*, 2023, **10**, 2250–2261

This journal is © the Partner Organisations 2023

Table 2 Formula and molecular mass of compounds

	Formula	MW (g mol^{-1})	ρ_P (cm^3 g^{-1})	$4S_M(S_M+1)$
Cu$_6$Zn	[Cu$_6$Zn(C$_5$H$_4$N$_5$)$_6$(OH)$_6$(OH$_2$)$_6$](SO$_4$)	1557	2.09	0
Cu$_6$Cu	[Cu$_6$Cu(C$_5$H$_4$N$_5$)$_6$(OH)$_6$(OH$_2$)$_4$](SO$_4$)	1520	2.08	3
Cu$_6$Ni	[Cu$_6$Ni(C$_5$H$_4$N$_5$)$_6$(OH)$_6$(OH$_2$)$_4$](SO$_4$)	1515	—	8
Cu$_6$Co	[Cu$_6$Co(C$_5$H$_4$N$_5$)$_6$(OH)$_6$(OH$_2$)$_6$](SO$_4$)	1551	2.11	15
Cu$_6$Cr	[Cu$_6$Cr(C$_5$H$_4$N$_5$)$_6$(OH)$_6$(OH$_2$)$_6$](SO$_4$)$_{1.5}$	1592	2.18	15

Accepting those two approximations implies that now there are only two variables: $4S_M(S_M+1)$ and $H\cdot\nabla(H_P)$. The remaining parameters in the formula can be simplified into A and B constant terms (eqn (4) and (5)) to lead to eqn (6):

$$[4S_M(S_M+1)] + 6\cdot[4S_{Cu}(S_{Cu}+1)]$$
$$= \frac{(\rho_P - \rho_S)\cdot g\cdot 8T\cdot MW}{\mu_0\cdot\rho_P\cdot H\cdot\nabla(H_P)} \quad (4)$$

$$[4S_M(S_M+1)] + A = \frac{B}{H\cdot\nabla(H_P)} \quad (5)$$

$$[4S_M(S_M+1)] = \frac{B}{H\cdot\nabla(H_P)} - A \quad (6)$$

Therefore, the experimental points at which the particles detach from the pole must fit to a straight line in a $4S_M(S_M+1)$ vs $1/[H\cdot\nabla(H_P)]$ plot. In order to check the validity of these equations, the magnetic field and its gradient were measured on the pole surface of the electromagnet at different current I values. Fig. 7 depicts the magnetic field measured along the plane corresponding to the surface of the magnetic pole in the vertical z-axis. The magnetic data were fitted to a fourth order polynomial expression, and ∇H and $H\cdot\nabla H$ were computed. The particles are sustained at the position where the upwards force is maximum; according to eqn (1), it corresponds to the position of the most negative $H\cdot\nabla H$ product: close to the lower end of the pole. Fig. 8 shows the dependence of the most negative $H\cdot\nabla H$ product for each current value with the magnetic field measured in the center of the pole.

From the experimental data shown in the $4S_M(S_M+1)$ vs $1/[H\cdot\nabla(H_P)]$ plot (Fig. 9a), the values lie in a straight line with a
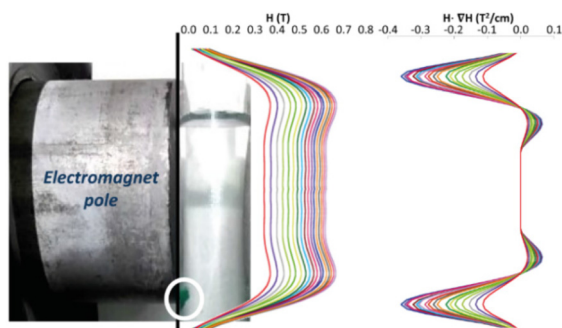

Fig. 8 $H\cdot\nabla(H)$ dependence on the magnetic field at the center of the pole. Left: second order polynomial fitting of the entire magnetic field range and right: linear fit within the range at which the experimental data appear for these compounds.

Fig. 9 Spin-term dependence with respect to $1/[H\cdot\nabla(H_P)]$ (a) and $1/H$ (b) values at which the particles are detached from the electromagnet pole when submerged in MeOH.

Fig. 7 Magnetic field profile [H and $H\cdot\nabla(H)$] on the electromagnet pole along the dashed line. The different colours refer to the applied intensity current: increasing from 0.0 to 2.5 A (step: 0.1 A).
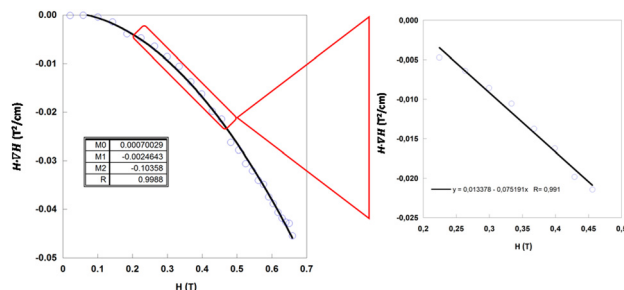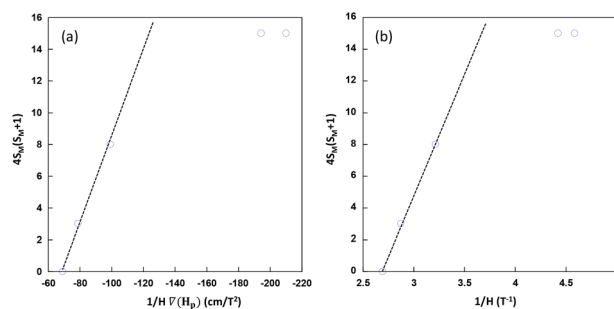
positive slope as predicted with the exception of **Cu$_6$Co** and **Cu$_6$Cr**. The first one is probably due to the well-known orbital contribution of Co^{II} that significantly deviates the spin-only susceptibility towards greater values. The second exception corresponds to **Cu$_6$Cr** whose magnetic coupling regime is closer to room temperature and it makes the spin only susceptibility calculation less realistic. It is noteworthy that at magnetic fields above 0.4 T, there is a linear relationship between ∇H and H (Fig. 9b); as a consequence the experimental data, all of them lying within this H region show also a linear correlation between $4S_M(S_M+1)$ and $1/H$.

Once it has been observed that these sustentation experiments provide a characteristic value for each compound depending on the total spin of the metal centers, it can be extended to the quantification of adsorbed molecules within the channels of these materials. Any increase of the particle

This journal is © the Partner Organisations 2023

Inorg. Chem. Front., 2023, **10**, 2250–2261 | **2257**

weight (due to a sorption phenomenon for example) will have a profound effect on the subtle balance between the magnetic attraction, gravity and buoyancy forces that determine the critical magnetic field at which the particles are detached from the poles of the electromagnet. Therefore, according to eqn (1)–(4) the modification of this critical value towards higher magnetic fields will indicate the sorption of the adsorbate molecules within the pores of the material. It has been exemplified by placing 15 mg of **Cu₆Cu** in 2 mL of an aqueous solution containing 15 mg of different adsorbates (or 15 μL if the adsorbate is liquid) for 12 hours at room temperature (25 °C) while gently stirred. Afterwards, the critical magnetic field is determined by placing these particles in a test tube attached to the pole of the electromagnet and containing distilled water. A film describing the experiment is provided in the ESI.†

The results are depicted in Fig. 10, where we can observe that **Cu₆Cu** presents both the selectivity based on the chemical nature of the adsorbates and also a size exclusion based selectivity. Chemical nature selectivity is observed for CH₃CN, DMSO and THF which provide negligible deviation with respect to the pristine **Cu₆Cu** compound (value indicated as Ø). These molecules are small enough to get into the pores of this material but do not interact strong enough to be adsorbed. In fact, the presence of adeninato molecules in the periphery of the heptameric entities makes this material well suited to strongly interact with molecules able to establish strong hydrogen bonding or π-stacking interactions. It becomes clear when observing a strong increase of the critical magnetic field measured for aniline, ribose and glucose. Besides, using a disaccharide (sucrose) and a trisaccharide

(raffinose), the size exclusion selectivity becomes evident, with no sorption at all for raffinose. A detailed study of the size and shape compatibility between the main void present in this compound (11.4 × 6.9 × 5.9 Å) and those of the adsorbate molecules helps understanding the different sorption capacity of **Cu₆Cu** toward the saccharides (Fig. S16†). The shapes of ribose (8.7 × 6.8 × 5.2 Å) and glucose (9.9 × 7.4 × 5.2 Å) monosaccharides fit relatively well inside this void leading to a high sorption capacity. In the case of sucrose disaccharide (11.2 × 9.1 × 6.7 Å), its dimensions are close or even slightly greater than the dimensions of the main void. However due to the flexibility of the supramolecular architecture and the conformational flexibility of sucrose it can accommodate into these voids but at the cost of a lower sorption capacity towards this adsorbate. Finally, in the case of raffinose trisaccharide (15.7 × 10.7 × 8.7 Å), its dimensions are far above those of the main void and no sorption is observed.

As is below described, the equations governing this phenomena (eqn 7, 8, 9 and 10) indicate a linear correlation between the adsorbed mass of guest molecules and the $H \cdot \nabla(H)$ product, in such a way that the greater the deviation with respect to the pristine critical magnetic value, the greater the mass of adsorbates captured by the porous material. To demonstrate this relation, we must separate the magnetic attraction force, gravitation and buoyancy in terms accounting for the framework of the compound (the heptameric entity plus the sulfate counterions) and for the adsorbates. The solvent molecules placed in the channels are not taken into consideration as previously stated.

$$\frac{\chi_M}{MW_F} \cdot \rho_F \cdot V_F \cdot H \cdot \nabla H = (V_F \cdot \rho_F + V_{Ads} \cdot \rho_{Ads}) \cdot g$$
$$- (V_F \cdot \rho_{H_2O} + V_{Ads} \cdot \rho_{H_2O}) \cdot g \quad (7)$$

$$\frac{\chi_M}{MW_F} \cdot \rho_F \cdot H \cdot \nabla H = (\rho_F - \rho_{H_2O}) \cdot g$$
$$+ (\rho_{Ads} - \rho_{H_2O}) \cdot \frac{V_{Ads}}{V_F} \cdot g \quad (8)$$

with V_F (ρ_F) and V_{Ads} (ρ_{Ads}) being the volume (density) occupied by the framework and the adsorbate in the particle. As $V_F = \frac{M_F}{\rho_F} = \frac{n \cdot MW_F}{\rho_F}$ and $V_{Ads} = \frac{M_{Ads}}{\rho_{Ads}} = \frac{n \cdot x \cdot MW_{Ads}}{\rho_{Ads}}$, then $\frac{V_{Ads}}{V_F} = \frac{x \cdot MW_{Ads} \cdot \rho_F}{MW_F \cdot \rho_{Ads}}$ (n being the times the framework formula is repeated in the particle and x is the relative ratio between the adsorbed guest molecules and the compound framework formula). As a consequence eqn (8) transforms into eqn (9):

$$H \cdot \nabla H = \frac{(\rho_F - \rho_{H_2O})}{\chi_M} \cdot \frac{MW_F}{\rho_F} \cdot g$$
$$+ \frac{(\rho_{Ads} - \rho_{H_2O})}{\chi_M} \cdot \frac{x \cdot MW_{Ads}}{\rho_{Ads}} \cdot g \quad (9)$$

In this latter equation, as all parameters except "$H \cdot \nabla H$" and "$x \cdot MW_{Ads}$" are constants (we assume that the ρ values of the

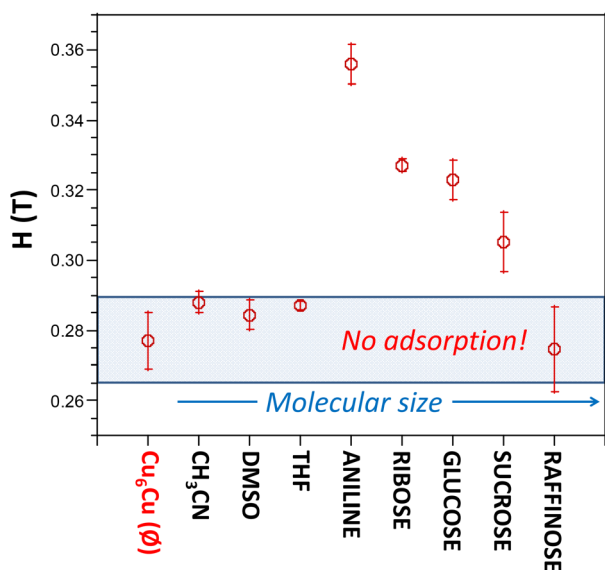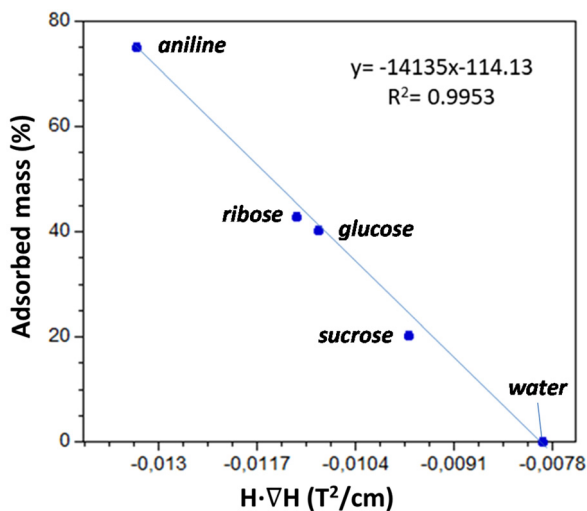**Fig. 10** Measured critical magnetic field at which the **Cu₆Cu** particles are detached from the pole of the electromagnet after the sorption experiment in aqueous solutions of a series of substances. Ø indicates control experiment using pure water.

2258 | *Inorg. Chem. Front.*, 2023, **10**, 2250–2261

This journal is © the Partner Organisations 2023

Fig. 11 Linear correlation between the adsorbed mass percentage and the $H \cdot \nabla(H)$ value at which the particles of the adsorbent are detached from the electromagnet pole.

different adsorbates are nearly the same), the above equation can be simplified to:

$$H \cdot \nabla H = A + B \cdot x \cdot MW_{Ads} = A + B \cdot M_{Ads} \qquad (10)$$

with M_{Ads} being the mass of the adsorbed molecules per formula of the framework compound. Therefore, there should be a linear relationship between the adsorbed mass and the $H \cdot \nabla H$ parameter at which the particles are detached from the pole of the electromagnet. The validity of this linear dependency has been checked by repeating the sorption experiments of aniline, ribose, glucose and sucrose using deuterated water and quantifying the amount of these adsorbates still in solution by ^{1}H-NMR (see further details in the ESI†). The representation of these values (in mass percentage with respect to **Cu$_6$Cu**) *vs* $H \cdot \nabla H$ fully validates the previous mathematical development (Fig. 11).

Conclusions

In summary, we have shown that it is possible to exploit the coordination environment diversity present in homometallic polynuclear entities to incorporate selected metal centers and tailor in this way the magnetic properties of the resulting heterometallic compounds. The room temperature magnetic response of these porous materials in the presence of external magnetic fields is strong enough to provide a novel sorption characterization technique. In this sense, the magnetic sustentation experiments that allow determining the minimum magnetic field required to attach these particles to the electromagnet pole provide a straightforward parameter that can be related to the amount of unpaired electrons and also to the density of the material. We have analyzed in depth the first of these parameters observing a linear correlation between $4S_M(S_M + 1)$ and $1/[H \cdot \nabla(H_P)]$ that can provide a new method to

estimate the susceptibility value of a compound if its density is known.

In a previous work, we exploited the variation of the second parameter (density) to monitor how $[Cu_6Cr(\mu\text{-adeninato-}\kappa N3{:}\kappa N9)_6(\mu_3\text{-OH})_6(\mu\text{-OH}_2)_6]^{3+}$ was able to capture an increasing amount of ibuprofen and naproxen anti-inflammatory drugs.[16] In this work, we have gone further being able to demonstrate the sorption selectivity of compound **Cu$_6$Cu** which showed a selectivity based on both the chemical nature of the adsorbate and its size. Finally, we just emphasize that this study has been performed directly in solution based on a property of the adsorbent and not as usually based on an indirect assessment by measuring the adsorbate remaining in solution.

Author contributions

The manuscript was written through contributions of all authors. These authors (R. P.-A., S. M.-G and J. P.-C.) contributed equally. All authors have given approval to the final version of the manuscript.

Conflicts of interest

There are no conflicts to declare.

Acknowledgements

References

1 K. S. Pedersen, J. Bendix and R. Clerac, Single-molecule magnet engineering: building-block approaches, *Chem. Commun.*, 2014, **50**, 4396–4415.

2 D. Maniaki, E. Pilichos and S. P. Perlepes, Coordination Clusters of 3d-metals that behave as single-molecule magnets (SMMs): synthetic routes and strategies, *Front. Chem.*, 2018, **6**, 461.

3 L. Bogani and W. Wernsdorfer, Molecular spintronics using single-molecule magnets, *Nat. Mater.*, 2008, 7, 179–186.

4 F. D. Natterer, K. Yang, W. Paul, P. Willke, T. Choi, T. Greber, A. J. Heinrich and C. P. Lutz, Reading and writing single-atom magnets, *Nature*, 2017, **543**, 226–228.

5 A. Dey, P. Bag, P. Kalita and V. Chandrasekhar, Heterometallic Cu^{II}–Ln^{III} complexes: Single molecule

magnets and magnetic refrigerants, *Coord. Chem. Rev.*, 2021, **432**, 213707.

6 D. Shao and X.-Y. Wang, Development of single-molecule magnets, *Chin. J. Chem.*, 2020, **38**, 1005–1018.

7 R. Sessoli, D. Gatteschi, A. Caneschi and M. A. Novak, Magnetic bistability in a metal-ion cluster, *Nature*, 1993, **365**, 141–143.

8 A. Zabala-Lekuona, J. M. Seco and E. Colacio, Single-molecule magnets: from Mn_{12}-ac to dysprosium metallocenes, a travel in time, *Coord. Chem. Rev.*, 2021, **441**, 2139842.

9 R. Pérez-Aguirre, G. Beobide, O. Castillo, I. de Pedro, A. Luque, S. Pérez-Yáñez, J. Rodríguez-Fernández and P. Román, 3D magnetically ordered open supramolecular architectures based on ferrimagnetic Cu/adenine/hydroxide heptameric wheels, *Inorg. Chem.*, 2016, **55**, 7755–7763.

10 J. Pascual-Colino, G. Beobide, O. Castillo, I. da Silva, A. Luque and S. Pérez-Yáñez, Porous supramolecular architectures based on π-stacking interactions between discrete metal-adenine entities and the non-DNA theobromine/caffeine nucleobases, *Cryst. Growth Des.*, 2018, **18**, 3465–3476.

11 J. Pascual-Colino, G. Beobide, O. Castillo, P. Lodewyckx, A. Luque, S. Pérez-Yáñez, P. Román and L. F. Velasco, Adenine nucleobase directed supramolecular architectures based on ferrimagnetic heptanuclear copper(II) entities and benzenecarboxylate anions, *J. Inorg. Biochem.*, 2020, **202**, 110865.

12 O. Kahn, Y. Pei and Y. Journaux, Orthogonality of the magnetic orbitals and ferromagnetic interaction, *Mol. Cryst. Liq. Cryst.*, 1989, **176**, 429–441.

13 T. Glaser, H. Theil, I. Liratzis, T. Weyhermüller and E. Bill, Ferromagnetic coupling by orthogonal magnetic orbitals in a heterodinuclear $(Cu^{II}V^{IV}) = O$ complex and in a homodinuclear $Cu^{II}Cu^{II}$ complex, *Inorg. Chem.*, 2006, **45**, 4889–4891.

14 W. Cai, J. D. Bocarsly, A. Gomez, R. J. Letona Lee, A. Metta-Magaña, R. Seshadri and L. Echegoyen, High blocking temperatures for DyScS endohedral fullerene single-molecule magnets. High blocking temperatures for DyScS endohedral fullerene single-molecule magnets, *Chem. Sci.*, 2020, **11**, 13129–13136.

15 J. Cirera, E. Ruiz, S. Álvarez, F. Neese and J. Kortus, How to build molecules with large magnetic anisotropy, *Chem. – Eur. J.*, 2009, **15**, 4078–4087.

16 R. Pérez-Aguirre, B. Artetxe, G. Beobide, O. Castillo, I. de Pedro, A. Luque, S. Pérez-Yáñez and S. Wutke, Ferromagnetic supramolecular metal-organic frameworks for active capture and magnetic sensing of emerging drug pollutants, *Cell Rep. Phys. Sci.*, 2021, **2**, 100421.

17 A. Earnshaw, *in Introduction to Magnetochemistry*, Academic Press, London, 1968.

18 *CrysAlis PRO*, Agilent Technologies, UK Ltd, Yarnton, England, 2011.

19 A. Altomare, M. Cascarano, C. Giacovazzo and A. Guagliardi, Completion and refinement of crystal structures with SIR92, *J. Appl. Crystallogr.*, 1993, **26**, 343–350.

20 L. J. Farrugia, WinGX suite for small-molecule single-crystal crystallography, *J. Appl. Crystallogr.*, 1999, **32**, 837–838.

21 G. M. Sheldrick, A short history of SHELX, *Acta Crystallogr., Sect. A: Found. Crystallogr.*, 2008, **64**, 112–122.

22 J. Cepeda, O. Castillo, J. P. García-Terán, A. Luque, S. Pérez-Yáñez and P. Román, Supramolecular architectures and magnetic properties of self-assembled windmill-like dinuclear copper(II) complexes with purine ligands, *Eur. J. Inorg. Chem.*, 2009, 2344–2353.

23 S. Pérez-Yáñez, G. Beobide, O. Castillo, J. Cepeda, A. Luque and P. Román, Structural diversity in a copper(II)/isophthalato/9-methyladenine system. From one- to three-dimensional metal-biomolecule frameworks, *Cryst. Growth Des.*, 2013, **13**, 3057–3067.

24 P. Van der Sluis and A. L. Spek, BYPASS: an effective method for the refinement of crystal structures containing disordered solvent regions, *Acta Crystallogr., Sect. A: Found. Crystallogr.*, 1990, **46**, 194–201.

25 A. L. Spek, Single-crystal structure validation with the program PLATON, *J. Appl. Crystallogr.*, 2003, **36**, 7–13.

26 J. Rodríguez-Carvajal, *FULLPROF 2000, Version 2.5d*, Laboratoire Léon Brillouin (CEA-CNRS), Centre d'Études deSaclay, Gif sur Yvette Cedex, Grenoble, France, 2003.

27 V. A. Blatov, A. P. Shevchenko and D. M. Proserpio, Applied topological analysis of crystal structures with the program package ToposPro, *Cryst. Growth Des.*, 2014, **14**, 3576–3586.

28 J. Krzystek, S. A. Zvyagin, A. Ozarowski, A. T. Fiedler, C. T. Brunold and J. Telser, Definitive spectroscopic determination of zero-field splitting in high-spin cobalt(II), *J. Am. Chem. Soc.*, 2004, **126**, 2148–2155.

29 J. Kobak, A. Bogucki, T. Smoleński, M. Papaj, M. Koperski, M. Potemski, P. Kossacki, A. Golnik and W. Pacuski, Direct determination of the zero-field splitting for a single Co^{2+} ion embedded in a CdTe/ZnTe quantum dot, *Phys. Rev. B*, 2018, **97**, 045305.

30 M. Idešicová, J. Titiš, J. Krzystek and R. Boča, Zero-field splitting in pseudotetrahedral Co(II) complexes: a magnetic, high-frequency and -field EPR, and computational study, *Inorg. Chem.*, 2013, **52**, 9409–9417.

31 R. T. Azuah, L. R. Kneller, Y. Qiu, P. L. W. Tregenna-Piggott, C. M. Brown, J. R. D. Copley and R. M. Dimeo, DAVE: a comprehensive software suite for the reduction, visualization, and analysis of low energy neutron spectroscopic data, *J. Res. Natl. Inst. Stand. Technol.*, 2009, **114**, 341–358.

32 D. Sonnenfroh and R. W. Kreilick, Exchange coupling in copper dimers with purine ligands, *Inorg. Chem.*, 1980, **19**, 1259–1262.

33 L. Cañadillas-Delgado, O. Fabelo, J. Pasán, F. S. Delgado, F. Lloret, M. Julve and C. Ruiz-Pérez, Unusual (μ-aqua)bis (μ-carboxylate) bridge in homometallic M(II) (M = Mn, Co and Ni) two-dimensional compounds based on the 1,2,3,4-butanetetracarboxylic acid: synthesis, structure, and magnetic properties, *Inorg. Chem.*, 2007, **46**, 7458–7465.

34 S. Pérez-Yáñez, O. Castillo, J. Cepeda, J. P. García-Terán, A. Luque and P. Román, Analysis of the interaction

2260 | *Inorg. Chem. Front.*, 2023, **10**, 2250–2261

This journal is © the Partner Organisations 2023

between adenine nucleobase and metal–malonato complexes, *Eur. J. Inorg. Chem.*, 2009, 3889–3899.

35 Y. Nishida and S. Kida, Crystal structures and magnetism of binuclear copper(II) complexes with alkoxide bridges. Importance of orbital complementarity in spin coupling through two different bridging groups, *J. Chem. Soc., Dalton Trans.*, 1986, 2633–2640.

36 V. McKee, M. Zvagulis and C. A. Reed, Further insight into magnetostructural correlations in binuclear copper(II) species related to methemocyanin: x-ray crystal structure of 1,2-.mu.-nitrito complex, *Inorg. Chem.*, 1985, **24**, 2914–2919.

37 Y. Z. Zheng, M. L. Tong, W. Xue, W. X. Zhang, X. M. Chen, F. Grandjean and G. J. Long, A "star" antiferromagnet: a polymeric iron(III) acetate that exhibits both spin frustration and long-range magnetic ordering, *Angew. Chem.*, 2007, **119**, 6188–6192.

38 K. C. Mondal, V. Mereacre, G. E. Kostakis, Y. Lan, C. E. Anson, I. Prisecaru and A. K. Powell, A strongly spin-frustrated FeIII7 complex with a canted intermediate spin ground state of S = 7/2 or 9/2, *Chem. – Eur. J.*, 2015, **21**, 10835–10842.

39 W. E. Hatfield, Superexchange interactions in copper(II) complexes, *ACS Symp. Ser.*, 1974, **5**, 108–141.

40 D. L. Lewis, K. T. McGregor, W. E. Hatfield and D. J. Hodgson, Preparation and structural and magnetic characterization of beta-di-u-hydroxo-bis[2-(2-dimethyl-aminoethyl)pyridine]dicopper(II) perchlorate, *Inorg. Chem.*, 1974, **13**, 1013–1019.

41 V. H. Crawford, H. W. Richardson, J. R. Wasson, D. J. Hodgson and W. E. Hatfield, Relation between the singlet-triplet splitting and the copper-oxygen-copper bridge angle in hydroxo-bridged copper dimers, *Inorg. Chem.*, 1976, **15**, 2107–2110.

42 J. Tercero, E. Ruiz, S. Alvarez, A. Rodríguez-Fortea and P. Alemany, Density functional study of magnetostructural correlations in cubane complexes containing the Cu_4O_4 core, *J. Mater. Chem.*, 2006, **16**, 2729–2735.

This journal is © the Partner Organisations 2023

Inorg. Chem. Front., 2023, **10**, 2250–2261 | **2261**